Effect of Various Impurities on Magnetite Deposition Behavior of Alloy 690TT Tube in PWR Secondary System

Soon-Hyeok Jeon[a,*], Ji-Min Lee[b], Hee-Sang Shim[a] ,Do Haeng Hur[a],
[a]*Materials Safety Technology Research Division, Korea Atomic Energy Research Institute, Daejeon, Korea*
[b]*Nucler R&D Policy Section, Korea Atomic Energy Research Institute, Daejeon, Korea*
[*]*Corresponding author: junsoon@kaeri.re.kr*

***Keywords :** Impurities, Sludge, Magnetite, Consolidation, Steam Generator, Alloy 690

1. Introduction

A steam generator (SG) is a main component of pressurized water reactors (PWRs), and its performance and integrity are managed by water chemistry control [1]. In particular, dissolved oxygen and pH control is the most important parameters that directly affects the material integrity in secondary system [2].

Meanwhile, the performance of secondary side of SGs could be severely degraded by the deposition of corrosion products and chemical impurities [3]. In PWR secondary system, flow accelerated corrosion (FAC) occurring in the feed train of a steam generator (SG) will lead to elevate iron concentration in the feedwater and form the iron oxide on feedwater piping and components [4,5]. After then, corrosion product particles are transported into the SGs from feedwater and deposited on the SG tube free span, top of tube sheet, and tube support plates. In addition, chemical impurities such as Na, Cl, and S can be introduced into the secondary system of a PWR owing to the condenser inleakage during the operation of a SG [6]. Chemical impurities can be concentrated within these magnetite piles by local boiling, which is called as hideout. This phenomenon can cause various SG degradation mechanism [6]. Sulfur and chloride ions can be responsible for pitting corrosion, stress corrosion cracking (SCC), and intergranular attack (IGA) [6]. In the case of Si, Al, and Ca, the deposits on top of tubesheets are consolidated or hardened by the formation of compounds containing impurities within the deposits [7]. This undesirable hard sludge can be detrimental because it is related to SG tube degradation by corrosion processes, such as outer diameter stress corrosion cracking (ODSCC) enhanced by the tube deformation or denting at the top of tubesheet.

There are many researches on impurities concentrated within the micro-pores of SG deposits. However, impurities related researches have mainly focused on the corrosion behavior of SG components in secondary water. However, in this study, the effects of various impurities on the magnetite deposition and consolidation related to deposit porosity of Alloy 690 thermally treated (TT) tubes were investigated using a magnetite deposition loop system. Among the various impurities, Na, Cl, Si, and Al were selected in this study because these impurities are frequently reported in actual SG tube deposits. Changes in the morphology, chemical composition of particles, and porosity of deposits on Alloy 690TT SG tube with/without the addition of impurities were evaluated using various analysis techniques.

2. Methods

2.1 Tube specimen preparation

Alloy 690TT SG tubes were cut with length of 500 mm, an inner diameter of 17.00 mm, an outer diameter of 19.05 mm, and thickness of 1.025 mm. One end of the specimens was blocked by welding with a cap of diameter of 19.05 and thickness of 2.0 mm. The chemical composition of Alloy 690TT tube used in this study is presented in Table I. A cartridge heater produced by stainless steel 316 was entirely covered with magnesium oxide and was inserted into the specimens. After drying at 60 ºC for 3 h, the outer surface of the specimen was cleaned with acetone, and the specimen was carefully installed in the test section.

Table I: Chemical composition of Alloy 690TT tube (wt. %).

Cr	Fe	Si	Mn	Ti	Al	C	Ni
29.3	10.4	0.3	0.3	0.3	0.2	0.02	Bal.

2.2 Magnetite deposition test

Fig. 1 shows a schematic of the magnetite deposition test loop used in this study. This system can closely simulate the secondary side conditions of SGs in PWRs. Deionized water of about 100 L was stored in a secondary coolant tank and recirculated by a high-pressure pump via a dissolved oxygen (DO) sensor, pH sensor, preheater, test section, heat exchanger, and back pressure regulator (BPR) with a flow rate of 260 mL/min. The concentration of DO was continuously maintained below 5 ppb during the deposition test. The pH of the circulating water was maintained at 9.5 by injecting diluted solutions of ethanolamine. Both the pH value and DO were continuously monitored using an in-situ sensor. The pressure of test section was then gradually increased to 60 bar by the BPR, and the water temperature near the tube surface was maintained at 270

°C to maintain subcooled nucleate boiling conditions by operating the pre-heater, ceramic heaters surrounding the test section, and the internal heater inside the Alloy 690TT tube specimen.

After test conditions were stabilized, iron sources were injected into the test section through the metering pump with a flow rate of 1 ml/min from the source tank. The precursor solution was diluted in the simulated secondary water stream and its final concentration was calculated as 0.7 ppm iron in the test section. In case of deposition test with NaCl addition, a mixed solution of Fe-acetate and NaCl was prepared in the iron source tank, and its final concentration in the test section was calculated to be 0.7 ppm Fe, 0.1 ppm Na, and 0.15 ppm Cl. In fact, the NaCl concentration was about 20 times higher than the recommended value, which is expected to show a more pronounced effect of NaCl [8]. Each magnetite deposition test with/without NaCl addition was conducted for 21 days.

In the case of test with Si and Al addition, Si and Al are injected in oxide form. However, when Si and Al are mixed with Fe-acetate in the source tank, they precipitate in the tank before conducting the deposition test. Hence, we firstly performed the magnetite deposition test without Si and Al addition for 14 days. After then, the sludge consolidation test was performed by addition of Si and Al impurities without iron sources for 14 days.

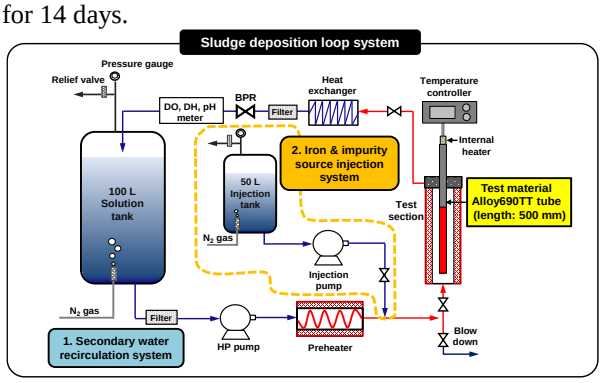

Fig. 1. Schematic of magnetite deposition loop system.

2.3 Microstructure of SG tube deposits

After the deposition tests, the SG tube specimens were cut into tubular segments for the measurement of magnetite mass and microstructural analysis of the magnetite. In case of deposition test with NaCl addition, to evaluate the amount of deposits, two tubular segments of about 20 mm in length at different axial locations were immersed separately in ethylenediaminetetraacetic (EDTA)-based solution at 93 °C for 12 hours to selectively dissolve the magnetite only. The dissolved solution was analyzed using an inductively coupled plasma (ICP) analysis to measure the iron concentration. Finally, the amount of magnetite per unit area was calculated by using the measured iron concentration.

In both cases, the deposits were analyzed by using a focused ion beam (FIB)-SEM to observe closely the cross-section of deposits. The deposit particle morphology, chemical composition, and deposit layer thickness were analyzed using FIB-SEM attached with an energy-dispersive X-ray spectroscopy (EDS).

In addition, the average two-dimensional porosity of the deposits was evaluated using at least seven cross-sectional SEM images. ImageJ software was used for porosity analyses.

3. Results and Discussions

3.1 Effect of NaCl addition on magnetite deposits

Fig. 2 shows the surface morphologies of the SG tube deposits without and with NaCl addition. Regardless of NaCl addition, the deposit particles are polyhedral or spherical in shape. The simulated particles are almost similar to the actual SG tube deposits [9,10]. However, it is observed that the particle size significantly decreases with the NaCl addition.

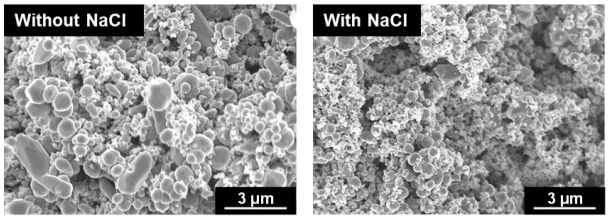

Fig. 2. Surface morphologies of the simulated deposits on SG tubes without and with NaCl addition using SEM analysis.

Fig. 3 shows the chemical composition of the deposit particles on the Alloy 690TT tubes with and without NaCl addition. Regardless of NaCl addition, the deposit particles are magnetite particles because they were composed of 53.56~55.92 at.% O and 44.08~46.44 at.% Fe.

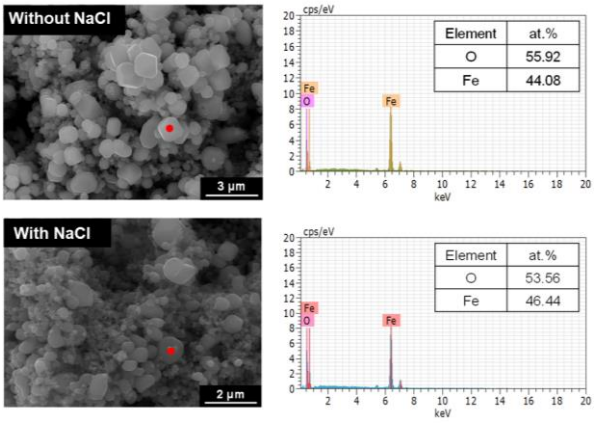

Fig. 3. Chemical composition of the simulated deposits on SG tubes without and with NaCl addition using SEM-EDS analysis.

Fig. 4 shows the cross-sectional SEM images of SG tube deposits without and with NaCl addition. Numerous micro-pores were clearly observed in the

deposits. Numerous pores are observed between the particles. The pores are created when steam bubbles escape from the heated metal surface and serve as accumulation sites for corrosive impurities [10].

Fig. 5 presents the two-dimensional porosity of the magnetite deposits depending on the NaCl addition. When NaCl is added, the porosity of deposits greatly decreases from 28.1% to 18.8%. The main reason of this observation is because the smaller particles have been accumulated densely. Considering that the thermal conductivity and hardness of deposits generally increases with the decrease in the porosity of the magnetite deposits, the denser magnetite deposits with the addition of NaCl may have a higher thermal conductivity [11] and hardness than that of the magnetite deposits without NaCl.

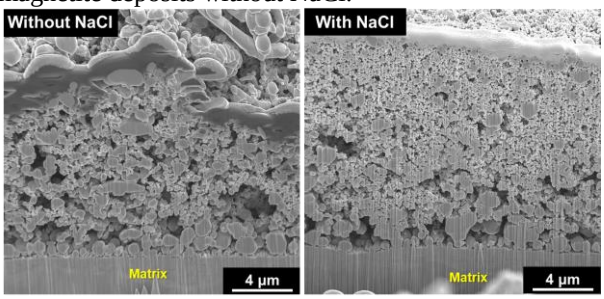

Fig. 4. Cross-section of the magnetite deposits on Alloy 690TT tubes without and with NaCl addition using SEM analysis.

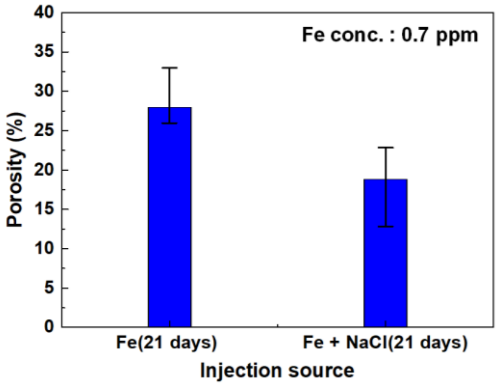

Fig. 5. Two-dimensional porosities of magnetite deposits depending on the NaCl addition using an image analyzer.

Fig. 6 shows the amount of magnetite deposits on Alloy 690TT tube per unit area depending on the addition of NaCl. Notably, the amount of magnetite deposits is greatly decreased by about 46% with the NaCl addition. This indicates that the impurities clearly affects the amount of magnetite deposited. The evaluation of magnetite zeta potential and surface zeta potential of Alloy 690TT tube depending on the NaCl is currently ongoing. Hence, the mechanism on the effect of NaCl addition on the magnetite deposition behavior of Alloy 690TT tube will be presented at the poster presentation.

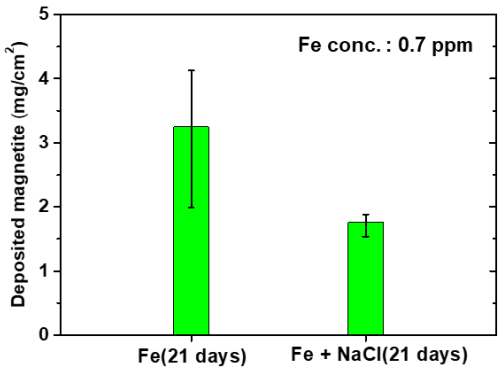

Fig. 6. Amount of magnetite deposits on Alloy 690TT tube per unit area depending on the NaCl addition.

3.2 Effect of Si and Al addition on magnetite deposits

Fig. 3 presents the surface morphologies of the SG tube deposits without and with Si and Al addition. Regardless of Si and Al addition, the deposit particles are polyhedral or spherical in shape. Various sized particles within the range of about 100 nm to 2 μm were present without Si and Al addition. However, it is observed that the particle size significantly decreases with the Si and Al addition.

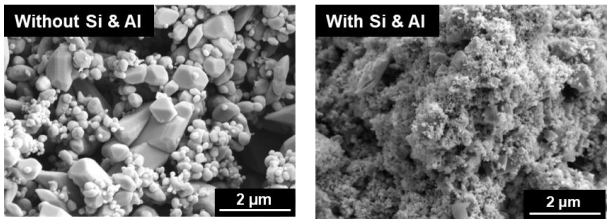

Fig. 7. Surface morphologies of the simulated deposits on SG tubes without and with Si and Al addition using SEM analysis.

Fig. 8 shows the chemical composition of the deposit particles on the Alloy 690TT tubes with and without Si and Al addition. In case of test without Si and Al addition, the deposit particles is magnetite particle. However, the deposit particle consisting of Fe, Al, and O was observed. This indicates that the Si and Al addition clearly affects the chemical composition of simulated deposit particles.

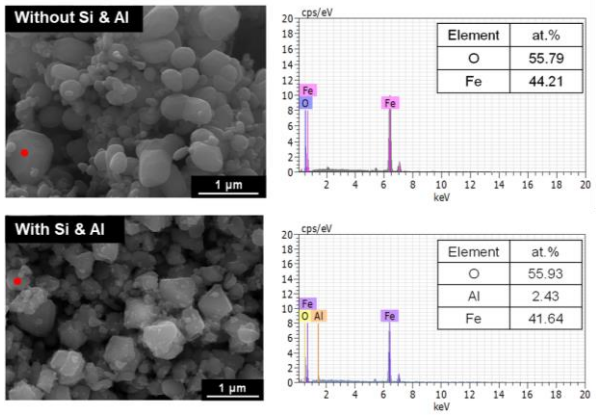

Fig. 8. Surface morphologies of the simulated deposits on SG tubes without and with Si and Al addition using SEM analysis.

Fig. 9 shows the cross-sectional SEM images of SG tube deposits without and with Si and Al addition. When Si and Al is added, the porosity of deposits greatly decreases.

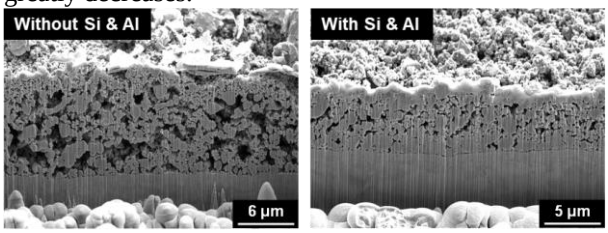

Fig. 9. Cross-section of the magnetite deposits on Alloy 690TT tubes without and with NaCl addition using SEM analysis.

Fig. 10 presents the two-dimensional porosity of the magnetite deposits depending on the Si and Al addition. When Si and Al is added, the porosity of deposits greatly decreases from 30.2% to 17.8%. As mentioned earlier, the main reason of this result is because the smaller particles have been accumulated densely. Considering that the consolidation of deposits generally increases with the decrease in the porosity of the magnetite deposits, the denser magnetite deposits with the Si and Al addition may have a higher hardness than that of the magnetite deposits without Si and Al addition.

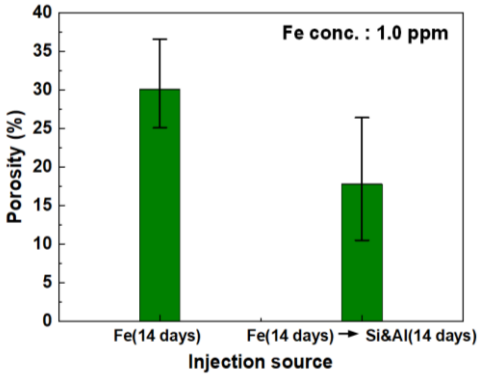

Fig. 10. Two-dimensional porosities of magnetite deposits depending on the NaCl addition using an image analyzer.

3. Conclusions

(1) Regardless of the addition of various impurities, the deposit particles are polyhedral or spherical in shape. However, the particle size significantly decreases with the addition of impurities.
(2) The porosity of the deposits with NaCl addition decreased about 33.1%, compared to the deposits without NaCl addition. The porosity of the deposits with Si and Al addition reduced approximately 42.1%, compared to the deposits without Si and Al addition. These results are because the smaller particles have been accumulated densely.
(3) Although impurities could increase thermal conductivity, they could increase the corrosion rate and sludge consolidation, so they must be carefully controlled in PWR secondary system.

ACKNOWLEDGEMENTS

This work was supported by the National Research Foundation (NRF) grant funded by the Korean government (NRF-2021M2E4A1037979 and RS-2022-00143316).

REFERENCES

[1] A. Drexler, Steam-water cycle chemistry relevant to nuclear steam generators, in: Steam Generators for Nuclear Power Plants, Chap. 6, Woodhead Publishing, 2017.
[2] C. Marks, Steam Generator Management Program: Effects of Different pH Control Agents on Pressurized Water Reactor Plant Systems and Components, Electric Power Research Institute (EPRI), EPRI report 1019042, 2009.
[3] C. W. Turner, K. Khumsa-Ang, Corrosion product transport and fouling in nuclear steam generators, in: Steam Generators for Nuclear Power Plants, Chap. 9, Woodhead Publishing, 2017.
[4] P. Franttini, Dispersants for Tube Fouling Control Volume 2: Short-Term Trial at ANO-2, EPRI TR-1003144, 2002.
[5] K. Fruzzetti, Multivariable Assessment of Flow Accelerated Corrosion and Steam Generator Fouling, EPRI TR-1003619, 2003.
[6] C. W. Turner, M. Huang, A. McKay, A., 2017. Hideout, hideout return and crevice chemistry in nuclear steam generators, in: Steam Generators for Nuclear Power Plants, Chap. 10, Woodhead Publishing, 2017.
[7] K. Beal, L. Million-Picallion, G. Lefèvre, G. Berger, S. Delaunay, C. Goujon, J.-L. Bretelle, Formation and consolidation of hard sludge under secondary circuit conditions. 20th NPC International Conference Brighton, 2016.
[8] K. Fruzzetti, Pressurized water reactor secondary water chemistry guidelines-Revision 8, Electric Power Research Institute (EPRI), EPRI report 3002010645, 2017.
[9] S.H. Jeon, H.S. Shim, J.M. Lee, J. Han, D.H. Hur, Simulation of Porous Magnetite Deposits on Steam Generator Tubes in Circulating Water at 270 ºC, Crystals, Vol. 10, p.729, 2020.
[10] S.H. Jeon, S. Hong, H.-C. Kwon, D.H. Hur, Characteristics of Steam Generator Tube Deposits in an Operating Pressurized Water Reactor. J. Nucl. Mater. 507, p.371, 2018.
[11] D.S. Smith, A. Alzina, J. Bourret, B. Nait-Ali, F. Pennec, N. Tessier-Doyen, K. Otsu, H. Matsubara, P. Elser, U. T. Gonzenbach, Thermal Conductivity of Porous Materials. J. Mater. Res. 28, p. 2260, 2013.